On-Chip Refractive Index Sensor With Ultra-High Sensitivity Based on Sub-Wavelength Grating Racetrack Microring Resonators and Vernier Effect

Li Liu [ID], Zhihao Hu, Mengyuan Ye [ID], Zhihua Yu [ID], Chenggong Ma, and Jian Li

Abstract—An approach to optimize the sensitivity and the limit of detection of on-chip refractive index sensor is proposed and demonstrated based on sub-wavelength grating racetrack microring resonator and Vernier effect. The sub-wavelength grating waveguide can reduce the structure limitation of the light field, which is beneficial to enhancing the interaction between the photon and analyte. By optimizing the parameters of the sub-wavelength grating racetrack microring resonator, the sensitivity of the sensor could be significantly improved to 664 nm/RIU. Subsequently, capitalizing the Vernier effect, a two cascaded microring-based refractive index sensor is designed. Owing to the Vernier effect, the wavelength spacings among the overlapped peaks could be effectively amplified more than ten times, leading to a high performance. The results demonstrate that an ultra-high sensitivity of 7061 nm/RIU and a low limit of detection of 1.74×10^{-5} RIU. With the advantages of ultra-high sensitivity and low limit of detection, the integrated device has important value in the fields of environmental monitoring and biosensors.

Index Terms—On-chip optical sensors, sub-wavelength grating microring, vernier effect, ultra-high sensitivity, low detection limit.

I. INTRODUCTION

IN RECENT years, owing to the dominant advantages of high refractive index contrast and complementary metal

Li Liu is with the School of Automation, China University of Geosciences, Wuhan 430074, China, with the Hubei Key Laboratory of Advanced Control and Intelligent Automation for Complex Systems, Wuhan 430074, China, with the Engineering Research Center of Intelligent Technology for Geo-Exploration, Ministry of Education, Wuhan 430074, China, with the State Key Laboratory of Chemo/Biosensing and Chemometrics, Hunan University, Changsha 410082, China, and also with the Key Laboratory of Optoelectronic Chemical Materials and Devices, Ministry of Education, Jianghan University, Wuhan 430056, China (e-mail: liliu@cug.edu.cn).

Zhihao Hu, Mengyuan Ye, Zhihua Yu, Chenggong Ma, and Jian Li are with the School of Automation, China University of Geosciences, Wuhan 430074, China (e-mail: zhihaohu@cug.edu.cn; yemy@cug.edu.cn; yuzhihua@cug.edu.cn; chenggongma@cug.edu.cn; jianli0228@cug.edu.cn).

Digital Object Identifier 10.1109/JPHOT.2022.3199908

oxide semiconductor (COMS)-compatibility [1], [2], [3]. many devices based on silicon-on-insulator (SOI) platform, have been utilized to design refractive index sensors, such as microdisk resonators [4], [5], [6]. microring resonators (MRR) [7], [8], [9], [10], [11], [12]. and photonic crystal cavities [13], [14], [15], [16]. In particular, microring resonators have been extensively investigated as silicon photonic refractive index sensors due to their design simplicity and ease of fabrication [17], [18]. However, the sensitivities of the refractive index sensors based on the ordinary strip MRRs are required to be improved because the interaction between the ordinary strip ring and the solution is not strong. To solve this dilemma, many researchers have proposed different optimization schemes for strip waveguide microrings. Ultra-thin waveguide microrings [7], Bragg grating microrings [19], [20]. slot waveguide microrings [21], [22], [23], and photonic crystal waveguide microrings [24], [25] are utilized to achieve refractive index sensors with sensitivities of 133 nm/RIU [7], 297 nm/RIU [19], 298 nm/RIU [23], and 200 nm/RIU [24], respectively.

The sub-wavelength grating (SWG) waveguide microrings [26], [27], [28] is a new type of silicon waveguide ring, which consists of periodic silicon pillars with a period smaller than the operating wavelength. As the contact area between the analytes and the waveguide ring is enlarged, it is very beneficial to enhance the interaction between the analyzed solution and photons. Consequently, the sensitivity could be improved. An SWG waveguide microring resonator (SWGMRR) realizes a sensitivity of 520 nm/RIU [29]. In the SWGMRR, effective sensing region includes not only the top and side of the waveguide, but also the space between the silicon pillars on the light propagation path, which is beneficial to enhancing the contact between light and medium. Another SWGMRR scheme based on the Fano resonance demonstrates a sensitivity of 366 nm/RIU [30]. A trapezoidal sub-wavelength grating waveguide microring resonator (T-SWGMRR) is proposed and the sensitivity of 440 nm/RIU is realized [31]. Considering the requirements of high-precision detection in biomedical science and environmental monitoring, it is still highly desirable to achieve a refractive index sensor with high sensitivity.

The Vernier effect has been widely utilized in optical sensors [32], which could effectively improve the sensitivities without requiring high-resolution measurement equipment. As the wavelength shift of the sensing measurement is generally
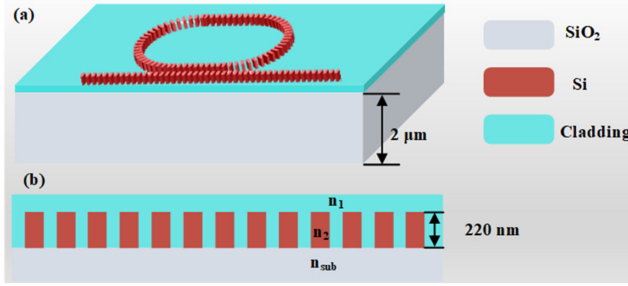
Fig. 1. (a) The structural diagram of SWGRMR, and (b) The structural diagram of SWG waveguide. n_{sub} is the index of the substrate, and n_1 and n_2 refer to the indexes of cladding and Si waveguide, respectively.

Fig. 2. (a) Top view of the SWGRMR. (b) Magnified view of the box region in (a), and (c) the basic unit of the SWG waveguide.

small, a narrow line width tunable laser or a high-resolution optical spectrum analyzer (OSA) is required [32]. In contrast, the Vernier effect is effective to reduce the equipment resolution requirement with maintaining high measurement precision. Even if the wavelength red-shift of the sensing resonance is small, the actual measured wavelength shift could be multiplied under the combined action of the sensing ring and the reference ring (i.e., Vernier effect), which contributes to the effective sensitivity improvement [32], [33], [34]. Consequently, by using the Vernier effect, a high-sensitivity refractive index sensor without requiring a narrow line width tunable laser or a high-resolution OSA could be obtained.

In this paper, a sub-wavelength grating waveguide racetrack microring resonator (SWGRMR) is optimized and further designed as a cascaded double-microring refractive index sensor based on the Vernier effect, which could obtain an ultra-high sensitivity. In this case, the sensitivity and the limit of detection (LOD) are improved to 7061 nm/RIU and 1.74×10^{-5} RIU, respectively. The high sensitivity is achieved with the solution refractive index ranging from 1.333 to 1.3405.

II. THEORETICAL DESIGN OF THE SWGRMR STRUCTURE

The structure of the SWGRMR is shown in Fig. 1(a), and the light cyan area represents the cladding region. Deionized waters doped with different concentrations of glucose solutions are used as the cladding material. The thick of the top silicon layer and the buried oxide layer are 220 nm and 2 μm, respectively, as shown in Fig. 1(b).

The structural parameters of the SWGRMR are labeled in Fig. 2. The pillar width, the bent waveguide radius, the racetrack length, the coupling gap, grating period and duty cycle of the racetrack microring resonator are denoted as W, R, L_c, G, Λ and f, respectively. The radius of the SWGRMR is chosen as R = 10 μm to guarantee low bending loss [35]. To make the SWG waveguide operate in the sub-wavelength regime ($\lambda/\Lambda > 2n_{eff}$, $\lambda = 1550$ nm), the period Λ is designed as 250 nm. Consequently, the light could propagate between the voids and the silicon pillars and avoid to be diffracted in the far field [36]. In order to realize the optimal sensing performance, the critical parameters of f, $W, G,$ and L_c are analyzed. The simulation conditions are set as follows. The mesh size, the light source, the wavelength range
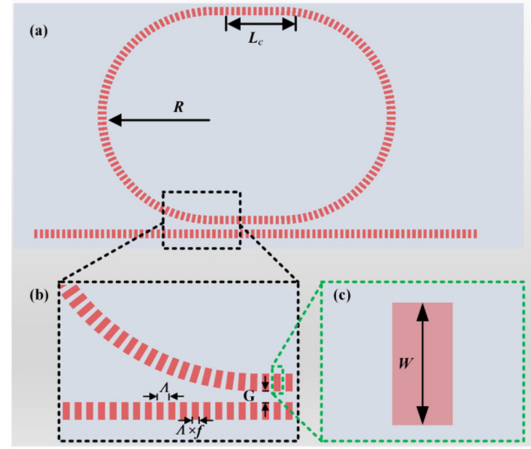
and simulation time are set as at least three, fundamental mode light source, 1500 nm $\sim$ 1600 nm and 300000 fs, respectively.

The device quality (Q) factor could be denoted by [27]

$$Q = \frac{\lambda_{res}}{\Delta\lambda_{FWHM}} \tag{1}$$

where λ_{res} is the resonant wavelength of the cavity, and $\Delta\lambda_{FWHM}$ is the full width at half maximum (FWHM) of resonant peak.

The sensitivity of the SWGMRR could be express as [37]

$$S_b = \frac{\Delta\lambda_{res}}{\Delta n_C} \tag{2}$$

where Δn_c is the refractive index change of the cladding solution, and $\Delta\lambda_{res}$ is the red-shifts of resonant wavelength.

Fig. 3(a) shows the transmission spectrum of the designed sensor with a duty cycle of 0.6. The free spectrum range (FSR) is 13.3 nm. The sensitivities of the SWGRMR refractive index sensor with different duty cycles are illustrated in Fig. 3(b). Deionized water was used as the initial cladding. The electric field distribution diagrams of SWG waveguide under different duty cycles are shown in Fig. 3(c)–(e). The refractive index of the glucose solution is ranging from 1.333 to 1.343 with a changing step of 0.0025. By varying the refractive index of the surrounding liquid, the shifts of the resonance peaks at different refractive indices could be measured to derive the sensitivity of the SWG ring. When the duty cycle is decreased from $f = 0.8$ to $f = 0.6$, the overlap region between the analyte and the light becomes larger, resulting in a stronger light-matter interaction. That is to say it is an effective method to improve the sensitivity of the sensor by reducing the duty cycle of SWG waveguide. It can be predicted that reducing the duty cycle will further improve the sensitivity. However, the larger propagation loss is caused by small duty cycle, which leads to the reduction of Q factor and the deterioration of LOD. Consequently, the duty cycle is designed as 0.6 to get a trade-off between the sensitivity and LOD.

The SWG waveguide width is also a key parameter affecting the sensitivity. The sensitivity (the blue line) and the Q factor
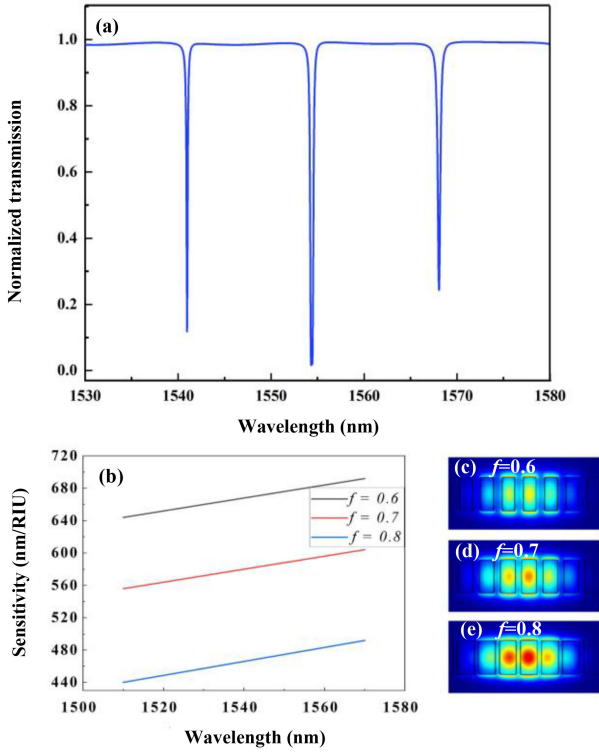
Fig. 3. (a) The transmission spectrum of the designed sensor with a duty cycle of 0.6, and (b) The sensitivities of the SWGRMR with different duty cycles. The electric field distribution diagrams of SWG waveguide under (c) f = 0.6, (d) f = 0.7, (e) f = 0.8, respectively.
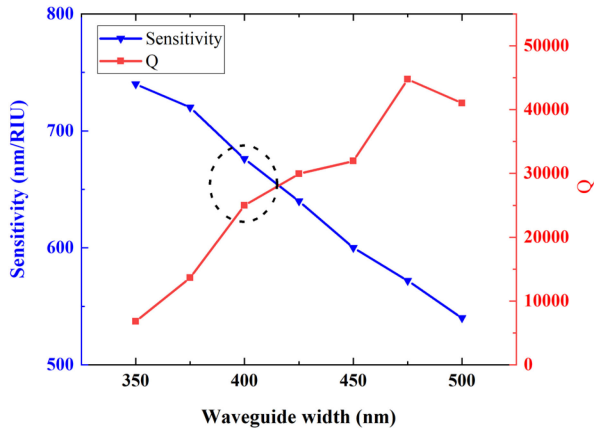

Fig. 4. The sensitivity and the Q factor of the SWGRMR under different waveguide widths.

(the red line) of the device under different widths are illustrated in Fig. 4. With the same SWG waveguide period and duty cycle, the waveguide width is optimized to simultaneously obtain a high sensitivity and a low LOD. With decreasing the waveguide width, the light limitation of the SWGRMR would be weaker, leading to a higher sensitivity and a lower Q factor. Hence the waveguide width W is chosen as 400 nm to balance the device sensitivity and LOD.

To investigate the relationship between the coupling gap G and the performance, the gaps are analyzed as follows. Fig. 5
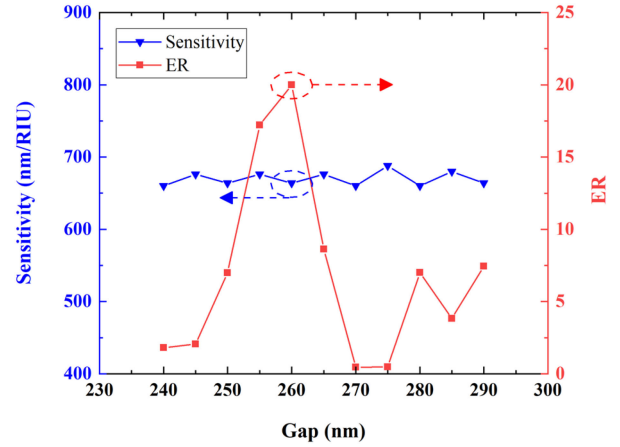

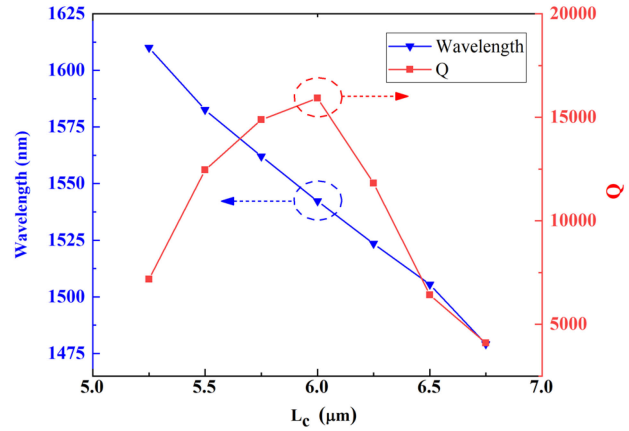Fig. 5. The sensitivity and the ER of the SWGRMR under different coupling gaps.

Fig. 6. The resonant wavelengths and the Q factors of the SWGRMR under different L_c.

shows the sensitivity (the blue line) and extinction ratio (ER) (the red line) under different gaps. With adjusting the gaps, the fluctuation range of the sensitivity could be neglected. On the contrary, when the gap G is set as 260 nm, the SWGRMR can realize the critical coupling and obtain the maximum ER, which is beneficial for the sensing measurement.

Fig. 6 illustrates the Q factor of the SWGRMR under different racetrack lengths (i.e., $L_c = 5.25~\mu m$, 5.5 μm, 5.75 μm, 6 μm, 6.25 μm, 6.5 μm, 6.75 μm). When L_c is chosen as 6.0 μm, the Q factor could realize the maximum value. In this case, the corresponding resonant wavelength is 1542.29 nm.

III. SENSING SCHEMES AND RESULT

A. Single-SWGRMR Sensor

Fig. 7 shows the initial transmission spectrum of the device in deionized water cladding. There are three resonance peaks (i.e.,1529.14 nm, 1542.29 nm, and 1555.73 nm). The ER of the peak at 1542.29 nm could realize 20 dB. As the Q factors corresponding to the three resonant peaks are 12190, 15918 and 10087 respectively, the resonant peak of 1542.29 nm (the red
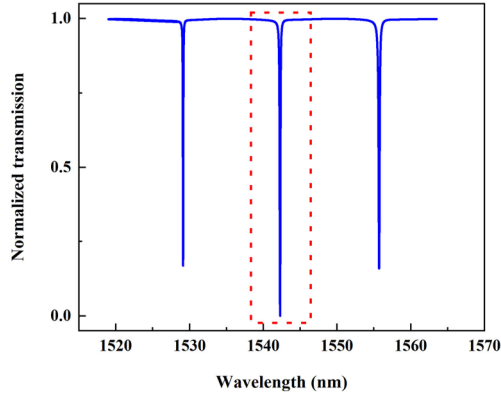
Fig. 7. Transmission spectrum of the SWGRMR with the deionized water cladding.

TABLE I
REFRACTIVE INDEXES OF THE GLUCOSE SOLUTIONS WITH DIFFERENT
CONCENTRATIONS AT 25 °C

Concentration	Refractive index
0g/100ml	1.333
2g/100ml	1.3355
4g/100ml	1.338
6g/100ml	1.3405
8g/100ml	1.343

dashed box) is chosen to verify the performance. As the effective refractive indices related to different wavelengths are not the same [29], the resonance FWHMs are different. According to the formula (1), the Q values corresponding to different wavelengths are different.

The initial cladding structure was deionized water at 25 °C. To explore the performance of the device in refractive index sensing, the cladding substance is selected as glucose solutions with different concentrations, whose refractive indexes at 25 °C are shown in Table I. The glucose solution is convenient to prepare a solution with a low refractive index change step. Moreover, it has no corrosive effect on the device, which would not affect the experimental results. By adjusting the concentration from 0g/100ml to 8g/100ml, the refractive index of the solutions could be tuned from 1.333 to 1.343.

The LOD of the sensor can be calculated by [38]

$$LOD = \frac{\lambda_{res}}{S_b \times Q} \quad (3)$$

where λ_{res} is the wavelength of resonance peak.

Fig. 8(a), shows the transmission spectra of the SWGRMR refractive index sensor in the glucose solutions with different concentrations. The initial transmission is illustrated as the black line with the central wavelength of 1542.29 nm (the black line, $n_1 = 1.333$). By increasing the refractive indexes of the solution, the device spectra would accordingly shift to 1543.96 nm (the red line, $n_2 = 1.3355$), 1545.62 nm (the blue line, $n_3 = 1.338$), 1547.27 nm (the green line, $n_4 = 1.3405$) and 1548.93 nm (the purple line, $n_5 = 1.343$), respectively. It means that a tiny change in refractive index can cause a significant shift in the wavelength of the resonant peak. By utilizing (1) and (2), the sensitivity and
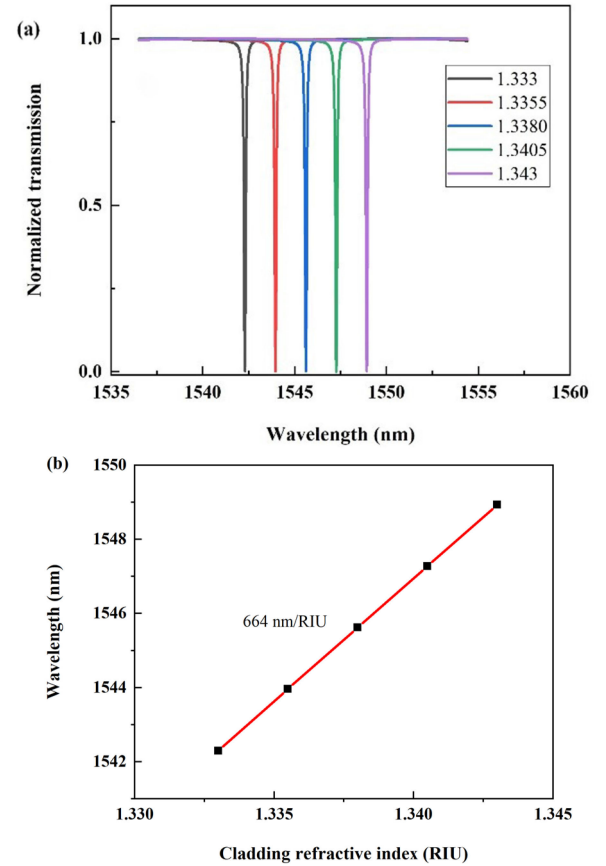

Fig. 8. (a) The transmission spectra of the SWGRMR refractive index sensor in the glucose solutions with different concentrations, and (b) The sensing performance of the single SWGRMR sensor.

LOD of the device are 664 nm/RIU (as shown in Fig. 8(b)) and 1.43×10^{-4} RIU, respectively. The three-dimensional finite-difference time-domain (3D-FDTD) method is used to verify the performance of the single ring sensor, and the difference compared with the MODE simulation results is acceptable, whose influence on the following sensor design incorporating with the Vernier effect is tolerable.

The sensitivities of the proposed SWGRMR sensor are compared to the other MRR-based schemes. On one side, the most sensitivities are lower than 520 nm/RIU [[26], [[27], [28], [29], [30], [31] while the sensitivity of the proposed sensor could realize 664 nm/RIU. On the other side, the most required fabrication precisions are about 50 nm [26], [27], [28] and the radii of the previous sensing rings are generally around tens of micrometers [27], [28], [29], [30], [31], [32], [33], [34]. In contrast, the required fabrication precision and the radius of the proposed sensing ring is 100 nm and 10 μm, respectively.

Moreover, the sensitivity in ref. [39] is very high, but our proposed sensor has some advantages. Firstly, the required fabrication precision of the subwavelength grating double slot waveguide resonator (GDSWGR) [39] is relatively high, as the two slot widths and the various pillar gaps are required to be 50 nm. Secondly, the maximum ER of the GDSWG is 9.4 dB and the operation wavelength is around 1700 nm. In contrast,
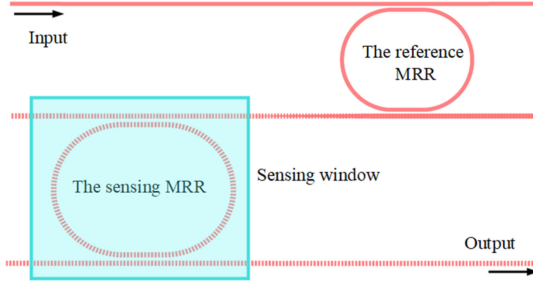
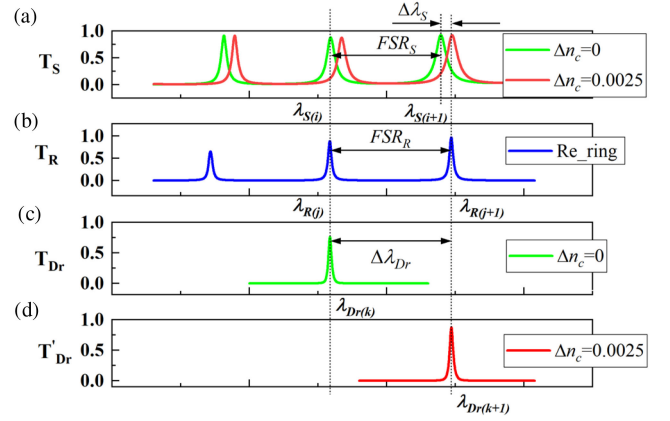Fig. 9. The schematic diagram of the cascaded double-microring sensor.

Fig. 10. (a) The transmission spectra of the sensing MRR in different concentration cladding solutions. (b) the transmission spectra of the reference MRR. The drop-port transmission spectra of the cascaded double-microring sensor when (c) $\Delta n_c = 0$ and (d) $\Delta n_c = 0.0025$.

the minimum feature size, ER and the operation wavelength of the propose sensor are 100 nm, 20 dB and around 1550 nm, respectively. The designed device structure does not have high requirements on the manufacturing process, which is required processing technology of 100 nm precision. Consequently, the proposed sensor could be fabricated on an SOI platform with fabrication methods compatible with CMOS foundry standards [40]. Furthermore, the proposed SWGRMR has a good manufacture tolerance on the sensing performance [41]. For instance, when the coupling gap of the sensing ring is changed around the optimum value of 30 nm, the sensitivity drops by at most 11%.

B. Cascaded Double-Microring Sensor

Although the sensitivity of the SWGRMR can be higher than 600 nm/RIU, the sensitivity of the single-microring-based refractive index sensor is difficult to exceed the order of 1500 nm/RIU. To solve the above problem, a new refractive index sensor is designed by a cascaded double-microring structure, including a sensing MRR (i.e., SWGRMR) and a reference MRR (a strip waveguide microring), as shown in Fig. 9. The reference ring is chosen as ordinary strip MRR to reduce the fabrication difficulty. The radius and the waveguide width are set as 5 μm and 400 nm, respectively. The coupling gap is designed as 160 nm to achieve a high ER and the racetrack length is chosen as 3 μm to obtain required FSRs and resonant wavelengths. As discussed in part II, the radius, the waveguide width, the grating period, the duty cycle, the coupling gap and the racetrack length of the sensing ring are chosen as 8 μm, 400 nm, 250 nm, 0.6, 260 nm and 6 μm, respectively. The taper length between the silicon waveguide and SWG waveguide is 20 μm. The output waveguide had better to be SWG waveguide to reduce the device loss. For the double-ring device, the FSR of the Vernier effect peaks is 179.89 nm.

During the verification process, the SWGRMR is exposed to a solution sample to detect the change of refractive index in the sensing window (i.e., the light blue box). The reference MRR can provide a stable comb transmission spectrum for the sensing MRR to achieve better sensing performance [32].

To obtain Vernier effect, the reference ring needs to be covered by the cladding and only the sensing ring is in the sensing window. If the reference ring and the sensing ring are simultaneously immersed in the liquid, the resonance peaks of the two rings would be both shifted. In this case, it is difficult to precisely

control the overlapping peak positions of the two MRRs, which might result in no Vernier effect.

Theoretically, the sensitivity of a microring resonator can be defined as

$$S_b = \frac{\lambda_{res}}{n_{eff}} \left(\frac{\partial n_{eff}}{\partial n_c} \right) \qquad (4)$$

here, λ_{res} is the central wavelength and n_{eff} is the refractive index of the waveguide.

In addition, when the cladding index changes, the n_{eff} of the SWG waveguide would be affected, which can be expressed as [34]

$$n_{eff} = n_{eff0} + \Delta n_{eff} = n_{eff0} + \Delta n_c \frac{\partial n_{eff}}{\partial n_c} \qquad (5)$$

where Δn_{eff} is the change of n_{eff}, due to the cladding index change Δn_c, and n_{eff0} is the initial value at the 25 °C.

The free spectrum ranges of the sensing MRR (FSR_S) and the reference MRR (FSR_R) are designed to be approximate ($FSR_S < FSR_R$). As shown in Fig. 10(a) and 10(b), when $\Delta n_c = 0$, the resonant wavelength $\lambda_{S(i)}$ of the sensing MRR overlaps with the resonant wavelength $\lambda_{R(i)}$ of the reference MRR. Hence the transmission spectrum of the cascaded double-microring exhibits one peak at $\lambda_{S(Dr(k))}$, shown as the green line in Fig. 10(c). When Δn_c is adjusted to 0.0025, the resonant wavelength of the sensing MRR would shift $\Delta \lambda_S$, which makes the resonant wavelength $\lambda_{S(i+1)}$ of the sensing MRR overlap with the resonant wavelength $\lambda_{R(j+1)}$ of the reference MRR. Consequently, the spectrum overlapped peak of the cascaded-microring moves from $\lambda_{Dr(k)}$ to $\lambda_{Dr(k+1)}$. Therefore, when Δn_c changes, the wavelength spacing between the two overlapped peaks of the cascaded microring could be denoted by

$$\Delta \lambda_{Dr} = \Delta \lambda_S + FSR_S = FSR_R \qquad (6)$$

The relationship between the changes of the cladding refractive index and the waveguide effective refractive index can be
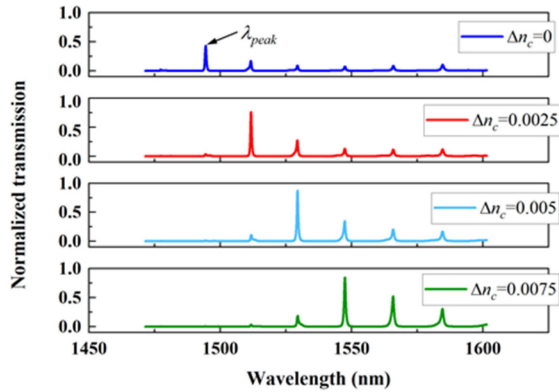
Fig. 11. The transmission spectra of the cascaded double-microring sensor in glucose solutions with different concentrations.

TABLE II
PERFORMANCE COMPARISON OF RECENT MICRORING REFRACTIVE INDEX
SENSORS WITH DIFFERENT TYPES OF WAVEGUIDES

Device	Sensitivity (nm/RIU)	LOD (RIU)	Radius (μm)
SWGMRR [29]	520	N/A	30
Fano-SWGMRR [30]	366	4×10^{-4}	5
T-SWGMRR [31]	440	N/A	10
Cascaded MRRs [32]	3456	1.15×10^{-2}	264
Cascaded MRRs [33]	5866	N/A	128/132/138
Slot MRR [42]	476	1.05×10^{-5}	30
SWGMRR [43]	600	N/A	10
Mid-infrared MRRs [44]	3000	2×10^{-3}	90/81
MRR-MZI [45]	3552	N/A	40
This work	7061	1.74×10^{-5}	8

expressed as

$$\Delta n_{eff} = \frac{\Delta \lambda_S}{\lambda_S(i)} n_{eff} = \frac{FSR_R - FSR_S}{\lambda_S(i)} n_{eff} \quad (7)$$

Then combining formulas (3)–(6), the whole device sensitivity S_{D_r} could be represented by

$$S_{Dr} = \frac{\Delta \lambda_{Dr}}{\Delta n_c} = \frac{FSR_R}{FSR_R - FSR_S} \frac{\partial n_{eff}}{\partial n_n} \frac{\lambda_s(i)}{n_{eff}} = FS_b \quad (8)$$

where $F = FSR_R/(FSR_R - FSR_S)$ is the amplification factor. Consequently, the sensitivity of the whole device could be amplified tens of times based on the Vernier effect of cascaded microrings.

The output transmission spectra of the sensor in glucose solutions with different concentrations (n_c: 1.333~1.3405) are shown in Fig. 11. $\Delta n_c = 0$ corresponds to deionized water (the refractive index is 1.333 at 25 °C), and the initial wavelength and Q factor of the overlapped peak are 1494.46 nm and 12500, respectively (the blue line). When the concentrations of the glucose solutions are set as 1.3355 ($\Delta n_c = 0.0025$), 1.338 ($\Delta n_c = 0.005$), and 1.3405 ($\Delta n_c = 0.0075$), the corresponding shifted peak wavelengths are 1511.78 nm (the red line), 1529.41 nm (the cyan line), and 1547.53 nm (the green line), respectively. Consequently, the sensitivity and the LOD of the sensor are 7061 nm/RIU and 1.74×10^{-5} RIU, respectively, which has distinguished advantages for high-resolution environmental monitoring and biosensor. Generally, the temperature change around the room temperature is relatively weak, thus the induced resonance red-shifts are small. Capitalizing the Vernier effect, the temperature influence on the sensing measurement could be significantly reduced. Moreover, the device temperature could be precisely controlled by utilizing a thermo electric cooler.

The performance of recent MRR-based refractive index sensors is shown in Table II. The sensitivities and LODs of the microring-based sensors are not higher than 600 nm/RIU [29], [30], [31], [42], [43]. and higher than 5×10^{-5} RIU [30], [32], [44], respectively. The sensitivities of the refractive index sensors can be significantly improved to 3456 nm/RIU [32], 5866 nm/RIU [33], 3000 nm/RIU [44] and 3552 nm/RIU [45] by two cascaded MRRs, three cascaded MRRs, mid-infrared MRRs and MRR-Mach Zehnder interferometer (MZI), respectively. However, the sizes of the above devices are relatively large [29], [32], [33], [42], [44], [45]. Compared with the above devices, the proposed cascaded double-microring sensor could realize an ultrahigh sensitivity (7061 nm/RIU) and a low LOD (1.74×10^{-5} RIU). In the future, the demonstrated sensor has great potential application value in on-chip optical systems [46], [47], [48], [49].

IV. CONCLUSION

In summary, we designed and verified an SWG-based refractive index sensor with ultra-high sensitivity and low detection limit. The parameters of the SWGRMR are analyzed and optimized to improve the sensing performance. Consequently, capitalizing the Vernier effect of the cascaded microrings, an ultra-high sensitivity of 7061 nm/RIU and a low LOD of 1.74×10^{-5} RIU could be simultaneously achieved. The key innovation in this manuscript is combining the designed compact SWGRMR and the Vernier effect, which could dramatically improve the sensitivity from hundreds of nm/RIU to thousands of nm/RIU. To the best of our knowledge, it is the highest sensitivity among the silicon-MRR-based schemes with such a small size, which is competent to be applied in high-resolution environmental monitoring and biosensor directions.

REFERENCES

[1] L. Liu, S. Liao, W. Xue, and J. Yue, "Tunable all-optical microwave filter with high tuning efficiency," *Opt. Exp.*, vol. 28, no. 5, pp. 6918–6928, 2020.

[2] S. M. Grist, S. A. Schmidt, J. Flueckiger, V. Donzella, W. Shi, and S. T. Fard, "Silicon photonic micro-disk resonators for label-free biosensing," *Opt. Exp.*, vol. 21, no. 7, pp. 7994–8006, 2013.

[3] L. Liu and X. Liu, "All-optical tunable microwave filter with ultra-high peak rejection and low-power consumption," *Opt. Exp.*, vol. 28, no. 9, pp. 13455–13465, 2020.

[4] X. Wang, X. Guan, Q. Huang, J. Zheng, Y. Shi, and D. Dai, "Suspended ultra-small disk resonator on silicon for optical sensing," *Opt. Lett.*, vol. 38, no. 24, pp. 5405–5408, 2013.

[5] L. Zhang and D. Dai, "Silicon subwavelength-grating microdisks for optical sensing," *IEEE Photon. Technol. Lett.*, vol. 31, no. 15, pp. 1209–1212, Aug. 2019.

[6] A. L. Moras et al., "Integrated photonic platform for robust differential refractive index sensor," *IEEE Photon. J.*, vol. 12, no. 5, Oct. 2020, Art no. 6802910.

[7] S. T. Fard et al., "Performance of ultra-thin SOI-based resonators for sensing applications," *Opt. Exp.*, vol. 22, no. 12, pp. 14166–14179, 2014.

[8] H. Sohlström, K. B. Gylfason, and D. Hill, "Real-time label-free biosensing with integrated planar waveguide ring resonators," *Proc. SPIE Silicon Photon. Photonic Integr. Circuits II*, vol. 7719, pp. 77190B–1–77190B–15, May 2010.

[9] D. Yang, B. Duan, X. Zhang, and H. Lu, "Nanoslotted microring resonator for high figure of merit refractive index sensing," *Opt. Appl.*, vol. 50, no. 1, pp. 37–47, 2020.

[10] G. Gao, Y. Zhang, H. Zhang, Y. Wang, Q. Huang, and J. Xia, "Air-mode photonic crystal ring resonator on silicon-on-insulator," *Sci. Rep.*, vol. 6, no. 1, pp. 1–6, 2016.

[11] E. Luan et al., "Enhanced sensitivity of subwavelength multibox waveguide microring resonator label-free biosensors," *IEEE J. Sel. Topics Quantum Electron.*, vol. 25, no. 3, May/Jun. 2019, Art no. 7300211.

[12] D. Urbonas, A. Balčytis, K. Vaškevičius, M. Gabalis, and R. Petruškevičius, "Air and dielectric bands photonic crystal microring resonator for refractive index sensing," *Opt. Lett.*, vol. 41, no. 15, pp. 3655–3658, 2016.

[13] S. Wang, Q. Cheng, J. Lv, and J. Wang, "Photonic crystal sensor based on Fano resonances for simultaneous detection of refractive index and temperature," *J. Appl. Phys.*, vol. 128, no. 3, pp. 034501–034507, 2020.

[14] M. Sovizil and M. Aliannezhadi, "Design and simulation of high sensitivity refractometric sensors based on defect modes in one dimensional ternary dispersive photonic crystal," *J. Opt. Soc. Amer. B*, vol. 36, no. 12, pp. 3450–3456, 2019.

[15] P. Saha and M. Sen, "Ultra-high Q-factor and ultra-sensitive refractive index sensor based on a multiple-slot photonic crystal cavity," *IEEE Trans. Instrum. Meas.*, vol. 70, 2021, Art no. 9504509.

[16] L. Y. Chiang, C. T. Wang, T. S. Lin, S. Pappert, and P. Yu, "Highly sensitive silicon photonic temperature sensor based on liquid crystal filled slot waveguide directional coupler," *Opt. Exp.*, vol. 28, no. 20, pp. 29345–29356, 2020.

[17] L. Liu, W. Xue, and J. Yue, "Photonic approach for microwave frequency measurement using a silicon microring resonator," *IEEE Photon. Technol. Lett.*, vol. 31, no. 2, pp. 153–156, Jan. 2019.

[18] L. Liu, J. Yue, X. Fan, and W. Xue, "On-chip passive optical diode with low-power consumption," *Opt. Exp.*, vol. 26, no. 25, pp. 33463–33472, 2018.

[19] C. Y. Zhao, L. Zhang, and C. M. Zhang, "Compact SOI optimized slot microring coupled phase-shifted Bragg grating resonator for sensing," *Opt. Commun.*, vol. 414, pp. 212–216, 2018.

[20] S. Heinsalu, Y. Isogai, Y. Matsushima, H. Ishikawa, and K. Utaka, "Record high sensitivity compact multi-slot sub-wavelength Bragg grating refractive index sensor on SOI platform," *Opt. Exp.*, vol. 28, no. 18, pp. 28126–28139, 2020.

[21] C. A. Barrios et al., "Slot-waveguide biochemical sensor," *Opt. Lett.*, vol. 32, no. 21, pp. 3080–3082, 2007.

[22] P. Steglich et al., "Hybrid-waveguide ring resonator for biochemical sensing," *IEEE Sensors J.*, vol. 17, no. 15, pp. 4781–4790, Aug. 2017.

[23] T. Claes, J. G. Molera, K. De Vos, E. Schacht, R. Baets, and P. Bienstman, "Label-free biosensing with a slot-waveguide-based ring resonator in silicon on insulator," *IEEE Photon. J.*, vol. 1, no. 3, Sep. 2009.

[24] Y. Xu, S. Hu, and M. Kong, "Air-mode photonic crystal micro-ring resonator with enhanced quality factor for refractive index sensing," *IEEE Photon. J.*, vol. 12, no. 3, Jun. 2020, Art no. 6601111.

[25] S. M. Lo, S. Hu, G. Gaur, Y. Kostoulas, S. M. Weiss, and P. M. Fauchet, "Photonic crystal microring resonator for label-free biosensing," *Opt. Exp.*, vol. 25, no. 6, pp. 7046–7054, 2017.

[26] L. Huang et al., "Improving the detection limit for on-chip photonic sensors based on subwavelength grating racetrack resonators," *Opt. Exp.*, vol. 25, no. 9, pp. 10527–10535, 2017.

[27] V. Donzella, A. Sherwali, J. Flueckiger, S. M. Griste, S. T. Fard, and L. Chrostowski, "Design and fabrication of SOI micro-ring resonators based on sub-wavelength grating waveguides," *Opt. Exp.*, vol. 23, no. 4, pp. 4791–4803, 2015.

[28] N. Wu and X. Li, "Side-mode suppressed filter based on an angular grating subwavelength grating microring resonator with high flexibility in wavelength design," *Appl. Opt.*, vol. 58, no. 26, pp. 7174–7180, 2019.

[29] J. Flueckiger et al., "Sub-wavelength grating for enhanced ring resonator biosensor," *Opt. Exp.*, vol. 24, no. 14, pp. 15672–15686, 2016.

[30] Z. Tu, D. Gao, M. Zhang, and D. Zhang, "High-sensitivity complex refractive index sensing based on Fano resonance in the subwavelength grating waveguide micro-ring resonator," *Opt. Exp.*, vol. 25, no. 17, pp. 20911–20922, 2017.

[31] H. Yan, L. Huang, X. Xu, S. Chakravarty, N. Tang, and H. Tian, "Unique surface sensing property and enhanced sensitivity in microring resonator biosensors based on subwavelength grating waveguides," *Opt. Exp.*, vol. 24, no. 26, pp. 29724–29733, 2016.

[32] L. Jin, M. Li, and J. J. He, "Highly-sensitive silicon-on-insulator sensor based on two cascaded micro-ring resonators with Vernier effect," *Opt. Commun.*, vol. 284, no. 1, pp. 156–159, 2011.

[33] Y. Liu, Y. Li, M. Li, and J. J. He, "High-sensitivity and wide-range optical sensor based on three cascaded ring resonators," *Opt. Exp.*, vol. 25, no. 2, pp. 972–978, 2017.

[34] C. Tian et al., "Temperature sensor of high-sensitivity based on nested ring resonator by Vernier effect," *Optik*, vol. 204, pp. 164118–164127, 2019.

[35] S. Xiao, M. H. Khan, H. Shen, and M. Qi, "Compact silicon microring resonators with ultra-low propagation loss in the C band," *Opt. Exp.*, vol. 15, no. 22, pp. 14467–14475, 2007.

[36] J. Wang, I. Glesk, and L. R. Chen, "Subwavelength grating devices in silicon photonics," *Sci. Bull.*, vol. 61, no. 11, pp. 879–888, 2016.

[37] N. L. Kazanskiy, M. A. Butt, and S. N. Khonina, "Silicon photonic devices realized on refractive index engineered subwavelength grating waveguides–A review," *Opt. Laser Technol.*, vol. 138, no. 1, pp. 106863–106874, 2021.

[38] E. Luan, H. Shoman, D. M. Ratner, K. C. Cheung, and L. Chrostowski, "Silicon photonic biosensors using label-free detection," *Sensors*, vol. 18, no. 10, pp. 3519–3561, 2018.

[39] N. L. Kazanskiy, S. N. Khonina, and M. A. Butt, "Subwavelength grating double slot waveguide racetrack ring resonator for refractive index sensing application," *Sensors*, vol. 20, no. 12, 2020, Art. no. 3416.

[40] Z. Ruan et al., "Releasing the light field in subwavelength grating slot microring resonators for athermal and sensing applications," *Nanoscale*, vol. 12, no. 29, pp. 15620–15630, 2020.

[41] L. Huang, H. Yan, L. Xiang, N. Zhou, D. He, and X. Mi, "Subwavelength racetrack resonators with enhanced critically coupled tolerance for on-chip sensing," *IEEE Access*, vol. 9, pp. 23424–23431, 2021.

[42] V. Mere, H. Muthuganesan, Y. Kar, C. Van Kruijsdijk, and S. K. Selvaraja, "On-chip chemical sensing using slot-waveguide-based ring resonator," *IEEE Sensors J.*, vol. 20, no. 11, pp. 5970–5975, Jun. 2020.

[43] Y. Xu, C. Fu, S. Sun, and M. Kong, "Wide-range refractive index sensing relied on tracking the envelope spectrum of a dispersive subwavelength grating microring resonator," *Opt. Laser Technol.*, vol. 154, Oct. 2022, Art no. 108304.

[44] Y. Chang, B. Dong, Y. Ma, J. Wei, Z. Ren, and C. Lee, "Vernier effect-based tunable mid-infrared sensor using silicon-on-insulator cascaded rings," *Opt. Exp.*, vol. 28, no. 5, pp. 6251–6260, 2020.

[45] Y. Zhang, J. Zou, Z. Cao, and J. J. He, "Temperature-insensitive waveguide sensor using a ring cascaded with a Mach-Zehnder interferometer," *Opt. Lett.*, vol. 44, no. 2, pp. 299–302, 2019.

[46] L. Liu, Y. Yang, Z. Li, X. Jin, W. Mo, and X. Liu, "Low power consumption and continuously tunable all-optical microwave filter based on an opto-mechanical microring resonator," *Opt. Exp.*, vol. 25, no. 2, pp. 960–971, 2017.

[47] L. Liu, H. Qiu, Z. Chen, and Z. Yu, "Photonic measurement of microwave frequency with low-error based on an optomechanical microring resonator," *IEEE Photon. J.*, vol. 9, no. 6, Dec. 2017, Art no. 5503611.

[48] D. Xiao et al., "Optical sensor network interrogation system based on nonuniform microwave photonic filters," *Opt. Exp.*, vol. 29, no. 2, pp. 2564–2576, 2021.

[49] L. Liu et al., "Low-power all-optical microwave filter with tunable central frequency and bandwidth based on cascaded opto-mechanical microring resonators," *Opt. Exp.*, vol. 25, no. 15, pp. 17329–17342, 2017.